

Analysis of Topological Transitions in Two-dimensional Materials by Compressed Sensing

Carlos Mera Acosta^{1,2}, Runhai Ouyang¹, Adalberto Fazzio^{2,3}, Matthias Scheffler¹, Luca M. Ghiringhelli¹, and Christian Carbogno^{1,*}

¹Fritz-Haber-Institut der Max-Planck-Gesellschaft, Faradayweg 4-6, 14195 Berlin-Dahlem, Germany

²Institute of Physics, University of Sao Paulo, CP 66318, 05315-970, Sao Paulo, SP, Brazil

³Brazilian Nanotechnology National Laboratory, CP 6192, 13083-970, Campinas, SP, Brazil

*carbogno@fhi-berlin.mpg.de

ABSTRACT

Quantum spin-Hall insulators (QSHIs), i.e., two-dimensional topological insulators (TIs) with a symmetry-protected band inversion, have attracted considerable scientific interest in recent years. In this work, we have computed the topological Z_2 invariant for 220 functionalized honeycomb lattices that are isoelectronic to functionalized graphene. Besides confirming the TI character of well-known materials such as functionalized stanene, our study identifies 45 yet unreported QSHIs. We applied a compressed-sensing approach to identify a physically meaningful descriptor for the Z_2 invariant that only depends on the properties of the material's constituent atoms. This enables us to draw a "map of materials", in which metals, trivial insulators, and QSHI form distinct regions. This analysis yields fundamental insights in the mechanisms driving topological transitions. The transferability of the identified model is explicitly demonstrated for an additional set of honeycomb lattices with different functionalizations that are not part of the original set of 220 graphene-type materials used to identify the descriptor. In this class, we predict 74 more novel QSHIs that have not been reported in literature yet.

In the last decade, the experimental realization of graphene and of topological insulators has fueled interest in the fundamental physics and possible applications that are hosted in linear band crossings. In fact, the crossing of energy bands in condensed matter has been investigated since the very early applications of formulation of quantum mechanics to periodic solids¹. Already in 1985, Volkov and Pankratov² showed that interfacing two semiconductors with mutually inverted bands can lead to massless Dirac fermions, i.e., linear electronic-dispersion relations that cross (leading to a phenomenon referred to as "band inversion") and connect conduction and valence bands. If this inversion occurs³ at time reversed pairs of reciprocal space points $\pm\vec{k}$, the respective boundary states associated to different spins must exhibit opposite momentum, which in turn forbids backscattering⁴⁻⁶. Quantum spin-Hall insulators (QSHI) are two-dimensional topological insulators (TIs)^{7,8} that intrinsically exhibit this property^{3,9}. In graphene, for instance, this band inversion is driven by spin-orbit coupling (SOC), which formally leads to a minute band-gap opening^{10,11}. In close analogy to charge pumping in the integer quantum-Hall effect¹², the spin charge pumped through the edge states is quantized in QSHIs¹³. The respective integer quantum, i.e., the topological Z_2 invariant, is 1 in QSHIs and 0 in trivial insulators. Formally, this Z_2 invariant is defined via the integral over the half Brillouin

zone (HBZ):

$$Z_2 = \frac{1}{2\pi} \left[\oint_{\partial\text{HBZ}} \mathbf{A}(\mathbf{k}) d\mathbf{l} - \int_{\text{HBZ}} \mathbf{F}(\mathbf{k}) d\tau \right] \mod (2) \quad (1)$$

of the Berry connection $\mathbf{A}(\mathbf{k})$ and Berry curvature $\mathbf{F}(\mathbf{k})$ ^{13,14}. This can be interpreted as the effective magnetic flux of a self-induced magnetic field, the Berry curvature, through the HBZ. Here, ∂HBZ is the contour of HBZ. Although theory predicted a wide variety of QSHIs^{4,5}, only few of them feature a large enough intrinsic bulk band gap at finite temperatures to allow for an experimental characterization, e.g., bilayer Bi^{15,16} as well as HgTe/CdTe^{17–19} and InAs/GaSb quantum wells^{20,21}.

So far, the computational search for new QSHIs has been a numerically costly trial-and-error process that required to compute the Z_2 invariant for each individual compound²². Since no simple rule of thumb exists that allows to *a priori* distinguish trivial from topological insulators²³, an “exhaustive search procedure seems out of reach at the present time”²⁴. Naturally, the search for new QSHIs was thus guided by experience and intuition, e.g., by focusing on heavy elements with high SOC^{25–28}. For instance, 17 potential TIs could be identified by carrying out high-throughput electronic band structure calculations for 60,000 materials²⁹. In the same spirit, high-throughput studies in this field have been performed using semi-empirical descriptors as a guidance, e.g., the derivative of the band gap with no SOC with respect to the lattice constant³⁰.

In this work, we focus on functionalized 2D honeycomb-lattice materials^{31–33}, a material class in which various QSHI candidates have been found already, e.g., functionalized stanene³⁴. By computing the Z_2 -invariant for 220 of these compounds from first principles we are able to identify 45 new QSHIs that have not yet been reported in literature. Using a recently developed statistical-learning approach^{35–37} based on compressed sensing, we then derive a two-dimensional “map” of these materials, in which metals, trivial insulators, and QSHIs are separated in different domains. The axes of this map are given by nonlinear analytic functions that only depend on the properties of the material’s constituent atoms, but not on the properties of the material itself. The identified descriptor captures the character of the electronic structure, revealing that orbital interactions can drive a band inversion even in compounds featuring relatively light elements and low SOC. Furthermore, we are also able to predict the topological character of materials without performing any additional first-principles calculations, just by evaluating their position on the “map”. By this means, we predict 74 additional novel QSHI candidates in a distinct material class, i.e., a set of different honeycomb lattice compounds with different functionalizations.

Results

First-principles Classification of Functionalized 2D Honeycomb-Lattice Materials

In a first step, we investigate the topological character of 220 functionalized 2D honeycomb-lattice materials ABX_2 (see Fig. 1) by computing their Z_2 invariant from first principles. We include all possible combinations AB that are isoelectronic with graphene (group IV-IV, III-V, and II-VI). For each honeycomb-lattice AB , functionalization with four different group VII elements (X either Cl, Br, F, or I) is considered. The resulting first-principles classification of these 220 compounds in metals (zero band gap), trivial insulators (nonzero band gap and $Z_2 = 0$), and QSHIs (nonzero band gap and $Z_2 = 1$) is shown in Fig. 1. 103 compounds are identified to be QSHIs in our calculations: In most cases (66%), the TI character is independent of the actual functionalization, as highlighted in blue in Fig. 1. These 68 functionalization-independent (FI) QSHIs consist of relatively heavy elements, feature topological band gaps between 5 meV and 2 eV, and include 15 new QSHIs and 53 QSHIs reported in literature before, e.g., functionalized stanene, germanene, Bi₂, GaBi, InBi, TlBi^{33,34,38–46}. Additionally, we also

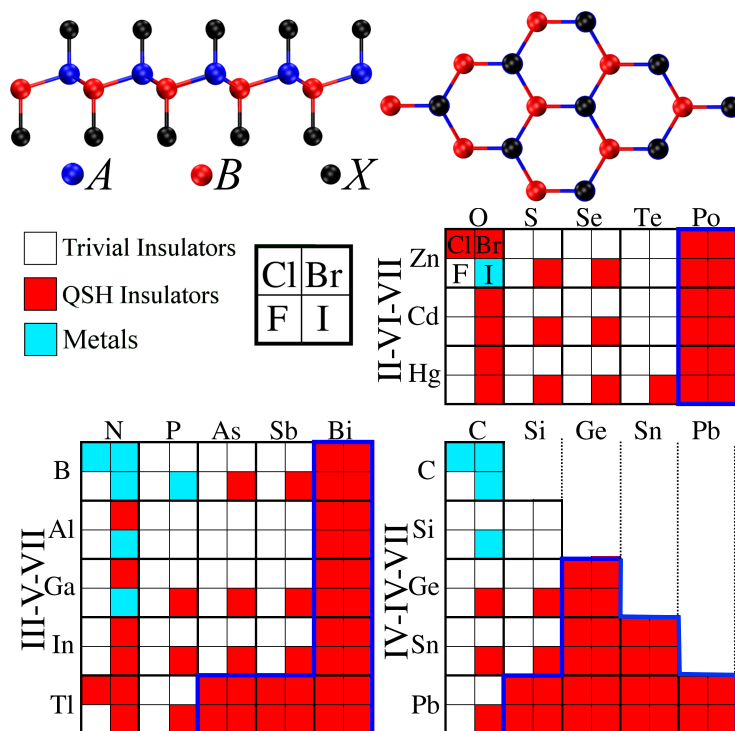


Figure 1. Side and top view of the functionalized honeycomb-lattice system. Classification (trivial insulators: white; QSHIs: red; metals: cyan) of the 220 investigated ABX_2 compounds. The x and y axes denote the A and B atoms. For each combination AB , the four individual squares correspond to a different functionalization with a group VII element (see legend). Compounds for which the topological character is independent of X are surrounded by a blue line. See Supp. Mat. for a tabulated list.

identify 35 QSHIs (34% of all QSHIs), for which the TI character depends on the actual functionalization (mostly iodides). These functionalization-dependent (FD) QSHIs with topological band gaps between 5 meV and 1 eV include 30 compounds that have not yet been reported in literature, e.g., AlNBr_2 and GaAsI_2 . Quite surprisingly, these TIs consist of relatively light elements with low SOC in the honeycomb lattice; they are however functionalized with relatively heavy atoms with strong SOC, which further substantiates that the topological transition is driven by the functionalization.

Descriptor Identification via Compressed Sensing

To identify descriptors that can *a priori* classify (i.e., the descriptor depends only on properties of the — isolated — atomic species constituting the material) functionalized 2D honeycomb-lattice materials in metals, trivial insulators, and QSHIs, we employed the SISSO (sure independence screening and sparsifying operator) approach recently developed by Ouyang *et al.*³⁷. First, a pool of about 10^7 different potential descriptors D_n is constructed by analytically combining the properties of the free atoms A , B and X computed with SOC (namely, the eigenvalues of the highest-occupied and lowest-unoccupied Kohn-Sham states ϵ^{ho} and ϵ^{lu} , the atomic number Z , the electron affinity EA, the ionization potential IP, and the size r_s , r_p , and r_d of the s , p , and d orbitals, i.e., the radii where the radial probability density of the valence s , p , and d orbitals are maximal. See Supp. Mat. for a full list including the values.). Second, this compressed-sensing-based technique identifies which low-dimensional combination of these descriptors represents the classification best, i.e., minimizes the overlap (or maximizes the separation)⁴⁷

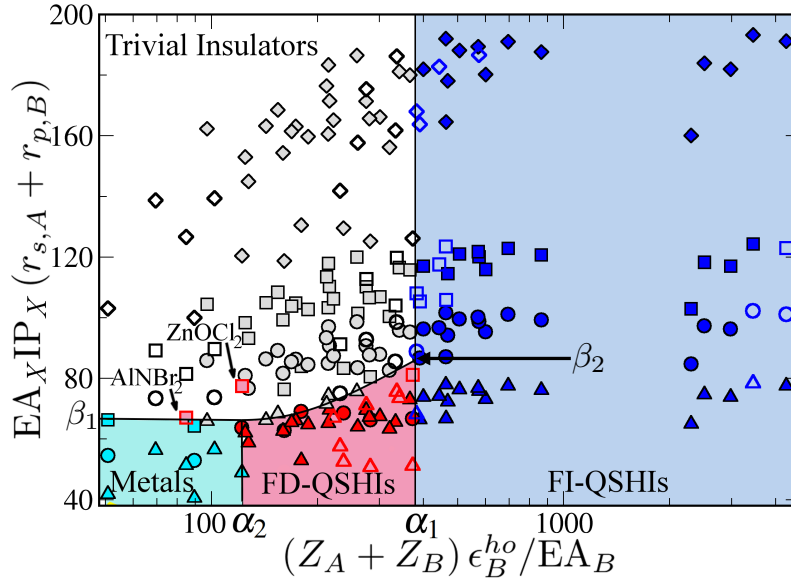


Figure 2. Representation of DFT result for the training (filled) and test (unfilled symbols) set in the domain defined by the two-dimensional descriptors. A logarithmic scale is used for D_1 . Compounds functionalized with F, Cl, Br, I are represented by diamonds, squares, circles and triangles, respectively. The symbols' color is used to distinguish between metals (cyan), FD-QSHIs (red), FI-QSHIs (blue), and trivial insulators (white/grey). The same color-code is used to highlight the different regions identified by the SISSO descriptors. The boundaries of the map of materials are defined by $\alpha_1 \approx 379$, $\alpha_2 \approx 122.1$, $\beta_1 \approx 70$, and $\beta_2 \approx 85$. The gap in the data points observed for $865 < D_1 < 2300$ is caused by the “jump” in Z_A and Z_B when switching from the 5th to the 6th row of the periodic system. See Supp. Mat. for a tabulated list.

among the convex hulls that envelope the individual classes (metals, trivial insulators, QSHIs). This procedure, which is performed for a “training” set (176 compounds randomly chosen from the total set of 220), reveals that the best descriptor for the classification of the investigated compounds is two-dimensional and features the components

$$D_1 = (Z_A + Z_B) \frac{\epsilon_B^{ho}}{EA_B} \quad (2)$$

$$D_2 = EA_X IP_X (r_{s,A} + r_{p,B}) . \quad (3)$$

For the remaining 20% of compounds, i.e., the so called “test” set used to validate the model, we find that all materials with a very well defined structural and topological character are correctly classified. Only $ZnOCl_2$ and $AlNBr_2$, which are both FD-QSHIs with minute band gaps (≤ 15 meV after SOC) at the verge of a topological transition to a trivial insulator or metal, respectively, are not correctly classified. This shows that the found descriptor, which exhibits a predictive ability greater than 95%, is robust and transferable, i.e., not limited to the original training set used to identify D_1 and D_2 .

As shown in Fig. 2, all compounds with $D_1 > \alpha_1$ are FI-QSHIs (blue). For $D_1 < \alpha_1$, the descriptor D_2 matters as well: Trivial insulators (white) occur for values of D_2 larger than the line connecting β_1 and β_2 , while for materials lying below that line we find metals (cyan) in the region $D_1 < \alpha_2$ and FD-QSHIs (red) for $\alpha_2 < D_1 < \alpha_1$. Note that D_1 and D_2 do not only clearly discriminate between metals, insulators, and QSHIs, but also separate FI-QSHIs from FD-QSHIs.

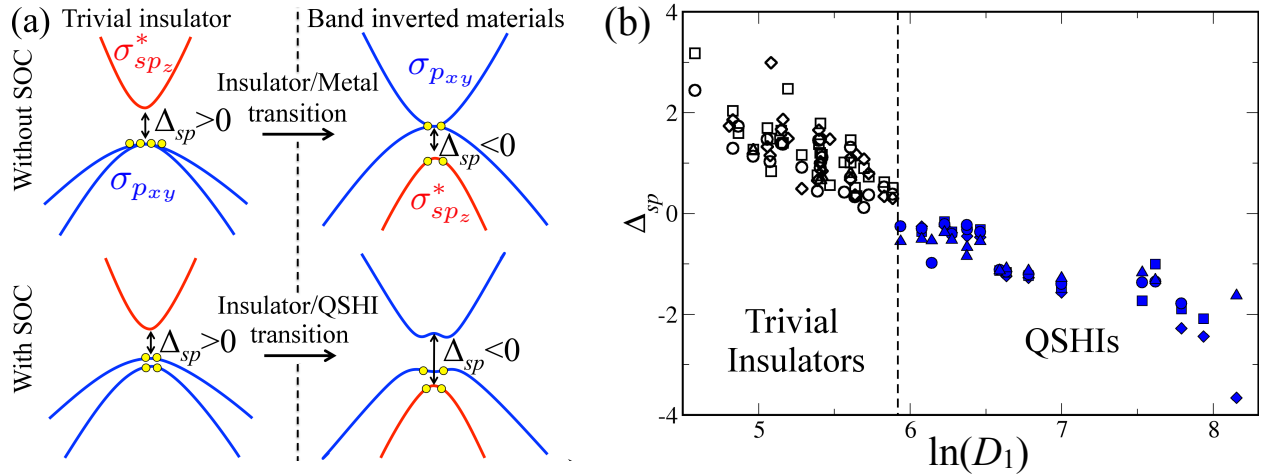


Figure 3. (a) Representation of the band structure with and without SOC for trivial insulators and band-inverted materials. Semimetals become insulators after including the SOC, leading to the QSHI phase. States formed by p_{xy} - (blue lines) and sp_z -orbitals (red lines) are inverted in the QSHIs; the energy distance between them (Δ_{sp}) is related to the robustness of the topological state, i.e., to which extent small perturbations such as strain can alter the topological character. The yellow dots represent four valence electrons; the four others accommodated in the bonding with the functionalization and the lower lying σ_s state are not shown. (b) Δ_{sp} as a function of the logarithm of D_1 for all FI-QSHIs and trivial insulators.

Qualitative Interpretation of the Results

The descriptor of components D_1 and D_2 does not only numerically and graphically sort the functionalized graphene-like materials, but also captures which atomic properties are relevant “actuators” for the topological phase transition. To understand this, it is necessary to clarify the character of the electronic states involved in the band inversion at Γ , as schematically sketched in Fig. 3a: These are the twofold degenerate $\sigma_{p_{xy}}$ state (blue), to which the two in-plane valence p_{xy} -orbitals from atoms B contribute, and the $\sigma_{sp_z}^*$ state (red), to which the valence s states from atoms A and the out-of-plane p_z states from atoms X contribute. Although all quantities entering Fig. 2 are computed with SOC, the descriptor (D_1, D_2) can be qualitatively rationalized as the relative energetic positions of these two states $\Delta_{sp} = E_{\sigma_{sp_z}^*} - E_{\sigma_{p_{xy}}}$ **before** SOC: If the twofold degenerate $\sigma_{p_{xy}}$ state lies lower in energy ($\Delta_{sp} > 0$), it is fully occupied, since it accommodates all remaining valence electrons. In this case, we get a trivial insulator, since the SOC can only lift the degeneracy of the $\sigma_{p_{xy}}$ state, but not invert the band order. Conversely, the $\sigma_{sp_z}^*$ state lies lower in energy for $\Delta_{sp} < 0$ and thus becomes fully occupied. With fewer remaining electrons, one thus gets a half-occupied $\sigma_{p_{xy}}$ state and so a band-inverted, semi-metal before SOC. The SOC itself is thus solely responsible for the band-gap opening, which leads to the QSHI state.

How the individual actuators present in the descriptor (D_1, D_2) influence the topological transition, can be qualitatively understood from their influence on Δ_{sp} . As shown in Fig. 3b, Δ_{sp} correlates linearly with $\ln(D_1)$ ($\Delta_{sp} \approx (-1.306 \pm 0.048) \ln(D_1) + (8.015 \pm 0.289)$) for functionalization-independent QSHIs. In this case, the influence of the p_z orbital of X on $\sigma_{sp_z}^*$ is negligible, so that Δ_{sp} is dictated by atoms A and B . The role of the actuators in the component D_1 of the descriptor can be rationalized using the tight-binding models developed for tetrahedral group IV and III-V semiconductors AB ^{48,49}. Here, ϵ_B^{ho}/EA_B captures

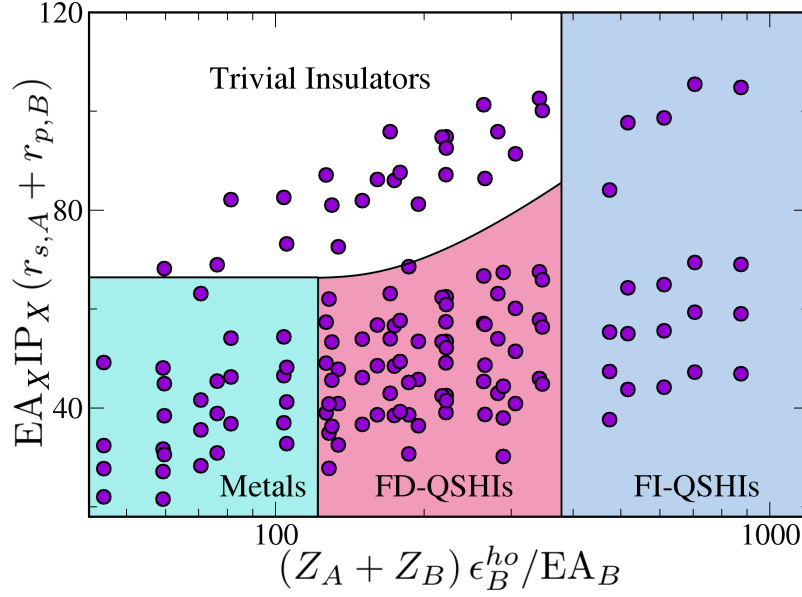


Figure 4. Representation of proposed V-V-VI and IV-VI-VI compounds in the domain defined by the two-dimensional descriptor components. See Supp. Mat. for a full list of the materials and their classification.

the energetic position of the hybridized p_{xy} -orbitals from atom B , whereas $(Z_A + Z_B)$ captures the size and thus the overlap of the respective orbitals. Just as in the case of tetrahedral semiconductors, heavier atoms lead to larger band widths and thus to reduced band gaps Δ_{sp} and metallic electronic structures.

Conversely, the component D_2 of the descriptor captures the influence of the functionalization. Due to its strong dependence on the electron affinity and ionization potential of atom X , it groups the compounds by functionalization for $D_1 > \alpha_1$, as apparent from Fig. 2. For $D_1 < \alpha_1$, however, it describes the actual stable geometry of ABX_2 and with that its electronic state: For light, strongly bound AB compounds such as BN and C_2 (small values of $Z_A + Z_B$ in D_1 and $r_{s,A} + r_{p,B}$ in D_2), only strongly electronegative atoms X (large values of $EA_X IP_X$) form a chemical bonding with AB , thus realizing a trivial insulators. Less electronegative functionalizations only physisorb via van-der-Waals interactions with AB , thus resulting in a metallic compound even after SOC. In this case, we also observe a structural transition from the so called low-buckled (LB) to the high-buckled structure⁵⁰. The insulator/metal transition with $D_2 < \beta_1$ and $D_1 < \alpha_2$ is thus essentially a LB-HB structural phase transition that is energetically favorable only in these particular compounds, as we explicitly checked. In particular, this holds for compounds with $D_1 > \alpha_2$ that are relatively close to a topological transition from the start. Here, the additional degree of freedom provided by the functionalization allows to tune the $\sigma_{sp_z}^*$ state. For strongly electronegative atoms X (large values of $EA_X IP_X$), this allows to close the gap Δ_{sp} and thus leads to a topological transition, as discussed in the context of Fig. 3a before.

To showcase that the gained insights and identified descriptors are transferable, we have computed D_1 and D_2 for 140 less common honeycomb ABX_2 compounds (AB from groups V-V and IV-VI functionalized with a group VI element for X). For these compounds, the identified descriptor predicts 20 FI-QSHIs, 54 FD-QSHIs, 42 trivial insulators and 24 metals, as shown in Fig. 4 and tabulated in the Supp. Mat.. Since $EA_X IP_X$ for X belonging to the VI group is lower, we get that the functionalization stabilizes the HB phase for non-QSHI materials. We have verified the prediction for selected compounds (AsX , SbX , $SnSeX_2$, $PSbX_2$, BiX and PO with $X: O, S, Se, Te$). It has been shown that oxide blue-phosphorene is a trivial insulator, which can become

a QSHI by applying tensile strain⁵¹. Recently, one compound has been reported as an intrinsic QSHI, AsO⁵². Different from individual systems proposed by trial-and-error calculations, the employed SISSO approach allows to identify a complete family of 74 new QSHI candidates.

Methods

First-principle calculations

For each of these systems, we have first determined the equilibrium lattice constant by relaxing both the atomic positions and the unit-cell shape until the residual forces on the atoms were smaller than 0.01 eV/Å using the all electron, full potential numeric atom centered orbitals based electronic structure code *FHI-aims*^{53–56}. For the equilibrium configuration, the topological invariant Z_2 was computed from the evolution of the Wannier center of charge^{24,57–59} that we implemented in *FHI-aims* using the band structures and wavefunctions. For these latter properties, SOC was accounted for using a second-variational, second-order perturbation approach recently implemented in *FHI-aims*⁶⁰ and first used in Ref.⁶¹. For a qualitative analysis of the band inversion mechanism, projected band structures were computed. All calculations were performed using the Perdew-Burke-Ernzenhof (PBE) generalized gradient approximation⁶², the Tkatchenko-Scheffler van der Waals correction method (DFT-TS)⁶³, and with numerical settings that guarantee a convergence of <1 meV for the eigenvalues. Specifically, periodic boundary conditions were used: the 2D hexagonal monolayers lie in the *xy*-plane, and a vacuum of 20Å was used in the *z*-direction to avoid the undesirable interaction between the periodic images of sheets. Furthermore, “really tight” numerical settings and basis sets as well as a $40 \times 40 \times 1 \vec{k}$ point grid for the Brillouin zone were used.

Statistical approach for identifying descriptors: Compressed Sensing

To learn a descriptor for the Z_2 -invariant material property, we employed the compressed-sensing approach recently developed by Ouyang *et al.*³⁷, which mainly consists of two steps: *i*) construction of feature space (potential descriptors) by building analytical functions of the input parameters (atomic properties with SOC, in the case studied here), by iteratively applying a set of chosen algebraic operators, up to a certain complexity cutoff (number of applied operators). The used input atomic parameters are the eigenvalues of the highest occupied and lowest unoccupied Kohn-Sham states ϵ^{ho} , ϵ^{lu} , the atomic number Z , the electron affinity EA, the ionization potential IP, and the size of the *s*, *p*, and *d* orbitals (r_s , r_p , and r_d), i.e., the radii where the radial probability density of the valence *s*, *p*, and *d* orbitals are maximal, for *A*, *B* and *X*. All these features were computed using perturbative SOC⁶⁰. Consequently, the feature space is formed by N vectors $\mathbf{D}_n = (D_{n,1}, D_{n,2}, \dots, D_{n,M})$, where $D_{n,m}$ is the n^{th} combination of atomic features, e.g., $(\epsilon_A^{ho} + \epsilon_B^{ho} + \epsilon_X^{ho})$, evaluated on the constituent atoms of the m^{th} ABX_2 compound. For more details about the feature space construction please refer to Ref.^{36,37}; *ii*) descriptor identification by a scheme combining sure independence screening and sparsifying operator, SISSO. SIS selects features \mathbf{D}_n , highly correlated with the Z_2 topological invariant property, which is formally written as a vector of the training values of Z_2 -invariant. Starting from the features selected by SIS, the SO looks for the Ω -tuples of features that minimizes the overlap (or maximize the separation)⁴⁷, among convex hulls enveloping subsets of data. The dimensionality Ω of the representation is set as the minimal that yields perfect classification of all data in the “training” set. In this work $\Omega = 2$ was found sufficient. This procedure is performed for a “training” set (176 compounds randomly chosen from the total set of 220); the remaining 20% are used as a “test” set to validate the found model.

Acknowledgments

We thank the financial support by FAPESP under Grant Agreement No. 2016/04496-9 and the European Union's Horizon 2020 research and innovation program under Grant Agreement No. 676580 with The Novel Materials Discovery (NOMAD) Laboratory, a European Center of Excellence. L.M.G. acknowledges funding from the Berlin Big-Data Center (Grant Agreement No. 01IS14013E, BBDC). This project has received funding from the European Research Council (ERC) under the European Union's Horizon 2020 research and innovation programme (Grant Agreement No. 740233, TEC1p).

Author contributions statement

C.M.A. performed the first-principles calculations and SISSO classification, C.M.A. and C.C implemented the Z_2 invariant, R.O., M.S., and L.M.G developed the SISSO approach, R.O. implemented it, M.S. and A.F. conceived the idea, and C.C supervised the calculations. All authors have discussed the scientific results and have written the paper.

References

1. C. Herring, Phys. Rev. **52**, 365 (1937).
2. B. Volkov and O. A. Pankratov, ZhETF Pisma Redaktsiiu **42**, 145 (1985).
3. C. L. Kane and E. J. Mele, Phys. Rev. Lett. **95**, 146802 (2005).
4. Y. Ren, Z. Qiao, and Q. Niu, Reports on Progress in Physics **79**, 066501 (2016).
5. L. Kou, Y. Ma, Z. Sun, T. Heine, and C. Chen, J. Phys. Chem. Lett. **8**, 1905 (2017).
6. J. Maciejko, T. L. Hughes, and S.-C. Zhang, Annual Review of Condensed Matter Physics **2**, 31 (2011).
7. M. Z. Hasan and C. L. Kane, Rev. Mod. Phys. **82**, 3045 (2010).
8. X.-L. Qi and S.-C. Zhang, Rev. Mod. Phys. **83**, 1057 (2011).
9. B. A. Bernevig and S.-C. Zhang, Phys. Rev. Lett. **96**, 106802 (2006).
10. C. L. Kane and E. J. Mele, Phys. Rev. Lett. **95**, 226801 (2005).
11. B. A. Bernevig and S.-C. Zhang, Phys. Rev. Lett. **96**, 106802 (2006).
12. D. J. Thouless, M. Kohmoto, M. P. Nightingale, and M. den Nijs, Phys. Rev. Lett. **49**, 405 (1982).
13. L. Fu and C. L. Kane, Phys. Rev. B **74**, 195312 (2006).
14. C. L. Kane and E. J. Mele, Phys. Rev. Lett. **95**, 146802 (2005).
15. Z. Liu et al., Phys. Rev. Lett. **107**, 136805 (2011).
16. I. K. Drozdov et al., Nat Phys **10**, 664 (2014).
17. B. A. Bernevig, T. L. Hughes, and S.-C. Zhang, Science **314**, 1757 (2006).
18. M. König et al., Science **318**, 766 (2007).
19. E. B. Olshanetsky et al., Phys. Rev. Lett. **114**, 126802 (2015).

20. I. Knez, R.-R. Du, and G. Sullivan, Phys. Rev. Lett. **107**, 136603 (2011).
21. C. Liu, T. L. Hughes, X.-L. Qi, K. Wang, and S.-C. Zhang, Phys. Rev. Lett. **100**, 236601 (2008).
22. N. Mounet et al., Nature Nanotechnology 2018 13:3 **13**, 246 (2018).
23. S. M. Young et al., Phys. Rev. B **84**, 085106 (2011).
24. D. Gresch et al., Phys. Rev. B **95**, 075146 (2017).
25. C. Weeks, J. Hu, J. Alicea, M. Franz, and R. Wu, Phys. Rev. X **1**, 021001 (2011).
26. C.-C. Liu, H. Jiang, and Y. Yao, Phys. Rev. B **84**, 195430 (2011).
27. C. M. Acosta, M. P. Lima, R. H. Miwa, A. J. R. da Silva, and A. Fazzio, Phys. Rev. B **89**, 155438 (2014).
28. M. Zhou et al., Sci. Rep. **4**, 7102 (2014).
29. M. Klintenberg, J. T. Haraldse, and A. V. Balatsky, Applied Physics Research **6**, 31 (2014).
30. K. Yang, W. Setyawan, S. Wang, M. B. Nardelli, and S. Curtarolo, Nature Materials **11**, 614 (2012).
31. M. C. Lucking et al., Phys. Rev. Lett. **120**, 086101 (2018).
32. Al Balushi Zakaria Y. et al., Nat Mater **15**, 1166 (2016).
33. F.-C. Chuang et al., Nano Letters **14**, 2505 (2014).
34. Y. Xu et al., Phys. Rev. Lett. **111**, 136804 (2013).
35. L. M. Ghiringhelli, J. Vybiral, S. V. Levchenko, C. Draxl, and M. Scheffler, Phys. Rev. Lett. **114**, 105503 (2015).
36. L. M. Ghiringhelli et al., New. J. Phys. **19**, 023017 (2017).
37. R. Ouyang, S. Curtarolo, E. Ahmetcik, M. Scheffler, and L. M. Ghiringhelli, arXiv:1710.03319 (2017).
38. C. Si et al., Phys. Rev. B **89**, 115429 (2014).
39. Ya-ping Wang et al., Applied Physics Letters **108**, 073104 (2016).
40. C. Niu et al., Phys. Rev. B **91**, 041303 (2015).
41. C.-C. Liu et al., Phys. Rev. B **90**, 085431 (2014).
42. Z. Song et al., NPG Asia Materials 2014 6:12 **6**, e147 (2014).
43. K.-H. Jin and S.-H. Jhi, Sci. Rep. **5**, 8426 (2015).
44. Y. Ma, Y. Dai, L. Kou, T. Frauenheim, and T. Heine, Nano Letters **15**, 1083 (2015), PMID: 25559879.
45. L. Li, X. Zhang, X. Chen, and M. Zhao, Nano Letters **15**, 1296 (2015), PMID: 25625786.
46. X. Li et al., Nano Research **8**, 2954 (2015).
47. A. F. Bialon, T. Hammerschmidt, and R. Drautz, Chemistry of Materials **28**, 2550 (2016).
48. E. Mooser and W. B. Pearson, Acta Crystallographica **12**, 1015 (1959).
49. W. A. Harrison, Phys. Rev. B **8**, 4487 (1973).
50. P. Rivero, J.-A. Yan, V. M. García-Suárez, J. Ferrer, and S. Barraza-Lopez, Phys. Rev. B **90**, 241408 (2014).

51. G. Yang et al., The Journal of Physical Chemistry C **121**, 12945 (2017).
52. Y.-p. Wang et al., Appl. Phys. Lett. **110**, 213101 (2017).
53. V. Blum et al., Computer Physics Communications **180**, 2175 (2009).
54. V. Havu, V. Blum, P. Havu, and M. Scheffler, Journal of Computational Physics **228**, 8367 (2009).
55. F. Knuth, C. Carbogno, V. Atalla, V. Blum, and M. Scheffler, Comp. Phys. Comm. **190**, 33 (2015).
56. K. Lejaeghere et al., Science **351** (2016).
57. R. Yu, X. L. Qi, A. Bernevig, Z. Fang, and X. Dai, Phys. Rev. B **84**, 075119 (2011).
58. A. A. Soluyanov and D. Vanderbilt, Phys. Rev. B **83**, 235401 (2011).
59. A. A. Soluyanov and D. Vanderbilt, Phys. Rev. B **83**, 035108 (2011).
60. W. P. Huhn and V. Blum, Phys. Rev. Materials **1**, 033803 (2017).
61. D. Shin et al., Chemistry of Materials **28**, 4771 (2016).
62. J. P. Perdew, K. Burke, and M. Ernzerhof, Phys. Rev. Lett. **77**, 3865 (1996).
63. A. Tkatchenko and M. Scheffler, Phys. Rev. Lett. **102**, 073005 (2009).